Tellus (2005), 57B, 28–39
Printed in UK. All rights reserved

TELLUS

Aerosol properties and their spatial and temporal variations over North China in spring 2001

By XIA XIANG-AO[1]*, CHEN HONG-BIN[1], WANG PU-CAI[1], ZONG XUE-MEI[1], QIU JIN-HUAN[1] and PHILIPPE GOULOUB[2], [1]*LAGEO, Institute of Atmospheric Physics, Chinese Academy of Sciences, Bejing, China;* [2]*LOA, Université des Sciences et Technologies de Lille, Lille, France*

(Manuscript received 12 January 2004; in final form 24 May 2004)

ABSTRACT

Aerosol properties and their spatial and temporal variations over North China were analysed based on ground-based radiometer data for spring 2001. On the basis of the retrievals from sun/sky radiance and broad-band radiation measurements at four AERONET stations and eight first-class radiation stations over North China, the analysis comprised a detailed description of aerosol loading, size and absorption in this period. The impact of dust events on aerosol properties over the downwind region was emphasized.

Heavy aerosol loading and notable temporal variation over North China were revealed by both datasets. The average aerosol optical depth at 750 nm at the eight radiation stations ranged from 0.32 in Ejinaqi to 0.68 in Beijing, with the averaged coefficient of variation being 70%. Aerosol optical depth was dominantly contributed to by dust over western China, with 68% (±5%) of aerosol optical depth at 550 nm being attributed to large dust aerosols. A dramatic increase in aerosol optical depth associated with the remarkable decrease in the Ångstrom wavelength exponent was observed in Beijing and Xianghe during the dust episode. This indicated that a huge number of large particles were emitted into the atmosphere during the dust period, with the result that the contribution to aerosol optical depth from coarse particles approached the value observed in the dust source region.

Anthropogenic pollution also frequently contributed to the high aerosol optical depth in Beijing and Xianghe, but this was characterized by fine particles, with more than 70% of aerosol optical depth at 550 nm being attributed to fine particles. Pure desert aerosol in Chinese dust source regions absorbs much less solar radiation than predicted by known aerosol models. The retrieved single-scattering albedo was around 0.98 (±0.01) and had little wavelength dependence, which is in agreement with the ground-based and satellite retrievals in other dust source regions. Contrarily, anthropogenic aerosol exhibits much stronger absorption in the urban region, with the single-scattering albedo ranging from 0.89 ± 0.04 (at 440 nm) to 0.83 ± 0.05 (at 1020 nm). Due to the large difference in the absorption between dust and anthropogenic aerosol, the consequence of the input of a large volume of dust aerosols is not only to enhance the aerosol loading but also to reduce the aerosol absorption. Retrievals in Beijing showed that the single-scattering albedo increased to about 0.90 and had little spectral dependence when anthropogenic pollution and a dust event together affected Beijing; as for the pure dust period, it ranged from 0.92 at 440 nm to 0.97 at 1020 nm. The significant decrease in the aerosol absorption due to the dust outbreak can result in a decrease in aerosol atmospheric heating efficiency; this warrants further research since the increasing trend of aerosol loading with strong absorption in China is supposed to play an active role in regional and global climate change and the hydrological cycle.

1. Introduction

Aerosol radiative forcing, via direct or indirect channels, remains one of the large uncertainties in climate modelling and the projection of future climate scenarios. Much attention has been paid to this issue and many measures have been taken in recent years, for instance the launch of the new generation of space-borne sensors designed especially for aerosol retrievals, and the execution of large-scale comprehensive field experiments that integrate *in situ* measurements, satellite retrievals and models to reduce the uncertainties in the calculation of climate forcing due to aerosol particles. However, a thorough regionally dependent understanding of the chemical, physical and radiative properties of aerosols and their spatial and temporal variations is still lacking (IPCC, 2001).

The Gobi and deserts over northwestern China and southern Mongolia comprise one of the major dust aerosol source regions in East Asia. Intense frontal activity, mostly in late winter and spring, provides a mechanism for the injection of

*Corresponding author.
e-mail: xxa@mail.iap.ac.cn

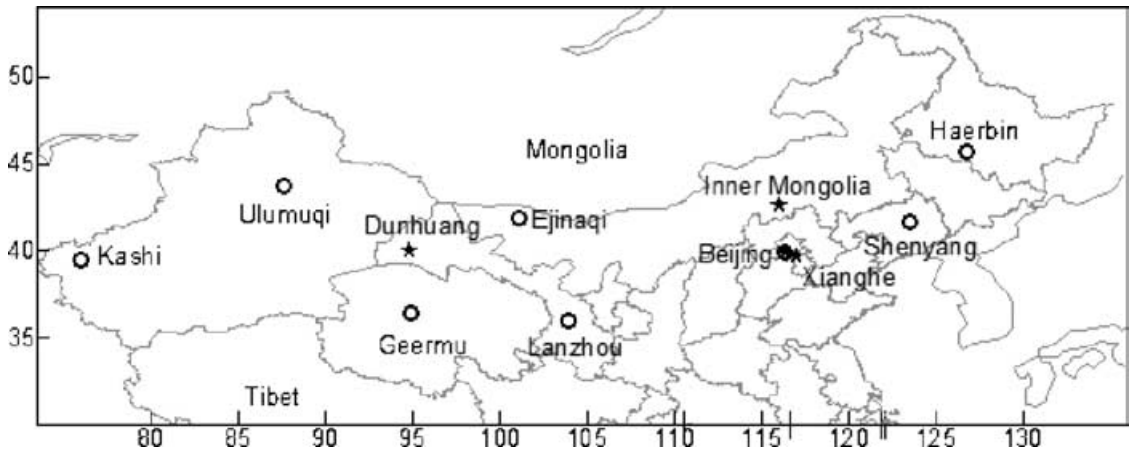

Fig 1. AERONET sites (stars) and radiation sites (circles) over North China used in this study. The Cimel sun/sky radiometer in Beijing is installed on the top of Institute of Atmospheric Physics Building (in a northern suburb); the pyrheliometer in Beijing is installed at Beijing Meteorological Observatory (in a southern suburb). The two sites are about 40 km apart. Xianghe is about 100 km from Beijing.

substantial amounts of material into the free troposphere and their transportation over long distances. On the other hand, the dramatic increase in industrial and agricultural activities, population and energy consumption in China has unavoidably been accompanied by a rapid increase in anthropogenic aerosols. As a consequence, the aerosols over northern China in spring comprise different types including sulfate, dust and soot, in a highly mixed condition, producing a complex aerosol loading in the troposphere. Chinese scientists have made substantial contributions to the observation and understanding of these aerosols and their effects. Wang et al. (2001) presented a detailed description of aerosol research in China, including the characterization of aerosols and the effect of aerosols on climate. However, systematic analyses of aerosol optical properties are still very rare, except for several papers focusing on only one or two locations or on one or two properties (Bergin et al., 2001; Qiu and Sun, 1994; Xu et al., 2002; Zhang et al., 2002).

Given the major advances in ground-based observation techniques and analysis methods, ground-based remote sensing of aerosols is best suited to the reliable and continuous derivation of detailed aerosol properties in key locations. This has had an active role in the characterization of key aerosol types: urban–industrial aerosol, biomass burning aerosol, desert dust and marine aerosol (Holben et al., 2001; Eck et al., 2003; Pinker et al., 2001; Smirnov et al., 2002). In spring 2001, four sunphotometer stations over northern China were established as a part of the AErosol RObotic NETwork (AERONET)—a ground-based aerosol monitor network. Solar spectral direct and diffuse radiances were collected during the first intensive observation period (IOP) of the Aerosol Characterization Experiment—Asia (ACE-Asia) project. This study attempts to present an initial understanding the complexity of aerosol properties by analysing AERONET data and combined aerosol optical depth (AOD) retrievals from eight first-class radiation stations over northern China, and hopes to facilitate aerosol modelling and aerosol remote sensing by satellite, etc. on the basis of the analysis. The paper is organized as follows. After a brief description of the experimental sites, measurements and data retrieval methods in the next section, Section 3 provides a general picture of the dust events in terms of AODs at eight radiation stations. Section 4 describes aerosol optical properties (AOD, Ångstrom wavelength parameter (ALPHA), aerosol size, absorption, etc.) on the basis of AERONET retrievals. Our conclusion and discussions are presented in Section 5.

2. Description of experimental sites and observations

In spring 2001, four AERONET stations (on which we focus our analysis) were established (Fig. 1, stars) in hyperarid (Dunhuang, DH), semiarid (Inner Mongolia, IM), urban (Beijing, BJ) and rural regions (Xianghe, XH) respectively. The sites are located in a nearly west–east transect of northern China. Figure 1 also presents eight first-class radiation observatories (circles). Note that they are mainly located in urban regions. A detailed description of each site is summarized in Table 1, the last column of which presents the number of days with AOD retrievals available for each month.

Solar spectral direct and scattered radiances are measured with the Cimel sun and sky scanning radiometer at AERONET stations. Holben et al. (1998) described the instrument and calibration in detail; here a brief description is given for completeness. The automatic tracking sun and sky scanning radiometer measures solar direct radiation with a 1.2° full field of view every 15 min at 340, 380, 440, 500, 675, 870, 940 and 1020 nm (nominal wavelengths). One set of measurements requires about 10 s, and measurements are taken in triplets at 30 s intervals. The direct radiance measurements are used to compute AOD at each

Table 1. Detailed description of AERONET and radiation sites. The final column shows the number of days with AOD retrievals available for each month

Station	Station description (location, elevation, climate, etc.)	Days
Dunhuang (DH)	40.04°N, 94.79°E; spring precipitation 6.9 mm; mean wind speed 2.7 m s^{-1}; mean temperature 11.7 °C; 1300 m above sea level; a tiny oasis surrounded by high mountains, desert and Gobi and at the west end of the Hexi Corridor, Gansu Province of China	March, 1 April, 17 May, 3
Inner Mongolia (IM)	42.68°N, 115.95°E; spring precipitation 11.5 mm; mean wind speed 4.2 m s^{-1}; mean temperature 3.7 °C; 1342 m above sea level; located in southern margin of Hunshandake Desert	April, 11 May, 9
Beijing (BJ)	39.98°N, 116.38°E; spring precipitation 64.1 mm; mean wind speed 3.2 m s^{-1}; mean temperature 12.9 °C; 92 m above sea level; Chinese capital with population over 10 million	March, 23 April, 19 May, 14
Xianghe (XH)	39.75°N, 116.96°E; rural region next to Beijing; elevation 36 m	March. 12 April, 13
Kashi	39.47°N, 75.98°E; spring precipitation 22.7 mm; mean wind speed 2.3 m s^{-1}; mean temperature 14.4 °C; 1289 m above sea level; located west of Taklimakan Desert	March, 21 April, 18 May, 23
Ulumuqi	43.78°N, 87.62°E; spring precipitation 85.3 mm; mean wind speed 2.9 m s^{-1}; mean temperature 7.9 °C; 918 m above sea level; site in urban area of Ulumuqi City, the capital of Xingjiang Autonomous Region	March, 28 April, 17 March, 24
Geermu	36.42°N,94.90°E; spring precipitation 7.3 mm; mean wind speed 3.5 m s^{-1}; mean temperature 6.1 °C; 2808 m above sea level; located in the south of Caidamu Basin	March, 28 April, 22 May, 28
Ejinaqi	41.95°N, 101.10°E; spring precipitation 7.6 mm, mean wind speed 2.3 m s^{-1}; mean temperature 14.4 °C; 941 m above sea level; located in the west of Inner Mongolia Autonomous Region	March, 24 April, 13 May, 23
Lanzhou	36.05°N, 103.90°E; spring precipitation 66.2 mm; mean wind speed 1.2 m s^{-1}; mean temperature 11.1 °C; 1517 m above sea level; site in urban area of Shenyang City, the capital of Gansu Province	March, 22 April, 14 May, 18
Shenyang	41.73°N, 123.50°E; spring precipitation 114.2 mm; mean wind speed 3.7 m s^{-1}; mean temperature 9.2 °C; 42 m above sea level; site in urban area of Shenyang City, the capital of Liaoning Province	March, 21 April, 20 May, 23
Haerbin	45.95°N, 126.77°E; spring precipitation 67.5 mm; mean wind speed 4.8 m s^{-1}; mean temperature 5.7 °C; 142 m above sea level; site in urban area of Haerbin City, the capital of Heilongjiang Province	March, 24 April, 22 May, 26

wavelength except for the channel at 940 nm, which is used to retrieve column-integrated water vapour content in centimetres. The Ångstrom wavelength parameter (ALPHA) is computed from AOD at 440 nm and 870 nm. Aerosol size distribution, refractive index and single-scattering albedo are inverted by the sky radiance almucantar measurements at 440, 670, 870 and 1020 nm with a combination of corresponding AODs. This is achieved by fitting the entire measured field of radiances to a radiative transfer model that is driven by the unresolved aerosol properties (Dubovik et al., 2000a). The AERONET data we present here are a level 2.0 quality-assured dataset (which is available from the AERONET website (http://aeronet.gsfc.nasa.gov/)). The data have been pre- and post-field calibrated, automatically cloud cleared (Smirnov et al., 2000) and manually inspected. The

Table 2. The retrieval accuracy for size distribution, $v(r)$, single-scattering albedo ω and refractive index $n - ik$ under the given conditions

$v(r)$	ω	n	k
10–25% for $0.1 < r < 7$ μm	0.03	0.04	30–50%
80–100% for the two edges	0.03	0.04	30–50%

inversion accuracies were determined by extensive sensitivity analyses and are listed in Table 2 (Dubovik et al., 2000b). A spheroid other than a sphere was used during the dust period in order to minimize non-spherical effects of dust on retrievals, such as artificial spectral dependence of the real part of the refractive index and artificially high concentrations of small particles (radius <0.1 μm) (Dubovik et al., 2002a).

On the basis of the sensitivity of total direct solar radiation (DSR) to aerosol optical parameters, Qiu (1998) proposed a parametrization model of DSR to derive AOD at 750 nm from DSR by a few iterations. Constraints on AOD retrievals by cloud, surface visibility and humidity measurements were introduced to minimize the cloud contamination (Qiu, 2003). As shown in numerical simulations and comparisons against sun-photometer observations, the error of AOD retrievals is less than 10%, and better accuracy may be achieved through averaging AOD spatially or temporally. The Chinese-made DFY-3 or TBS pyrheliometer was used to measure DSR at Chinese radiation stations. This pyrheliometer has a typical spectral response of 0.3–4 μm, a field of view angle of $3^\circ 21'$ or $4^\circ 24'$ and a yearly sensitivity stability of $\pm 1\%$. AODs are retrieved by hourly DSR measurements using Qiu's method if cloud and visibility constraints are satisfied and cloud cover observed at 08:00, 14:00 and 20:00 LST is less than 20%; then the daily averages are computed.

3. Dust events in terms of AOD inverted from broad-band measurements

Figure 2 presents the scatter plot between hourly AODs derived from spectral radiance and DSR in BJ (note that the two radiometers are spaced about 50 km apart). AERONET AODs at 750 nm were derived from a second-order polynomial fit to the logarithm of AOD versus the logarithm of wavelength. The hourly AERONET AOD average is computed from one to five observations corresponding to the observation time of DSR. A fair agreement between both derivations was evident, with a correlation coefficient of 0.93 and root mean square error (δ) of about 0.10. The linear correlation may be improved if a few questionable points are excluded, which is supported by the linear analysis of only those data points with AERONET AOD less than 0.6. At the present time we have no explanation for these questionable points. Perhaps, the important thing is that the majority of AOD retrievals from DSR data agree with those from AERONET very well.

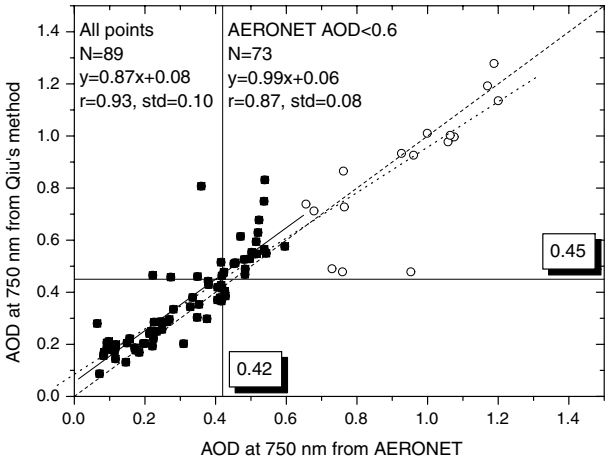

Fig 2. The linear regression analysis between hourly AOD retrievals from the method of Qiu (2003) and AERONET observations in Beijing. The dashed line represents a 1:1 relation. The dotted and solid lines represent fits on the bases of all data points and only the points with AERONET AOD < 0.6 (solid), respectively. The vertical and horizontal solid lines denote the overall AOD averages (AERONET 0.42; broad-band method 0.45).

The daily AODs at 750 nm at eight radiation stations are presented in Fig. 3. The broken line depicts the overall AOD average. As described in Table 1, five out of eight stations are located in the capital cities, and Kashi and Geermu are also industrial centres of western China; only Ejinaqi is located in a small county. This is not unique to China, however; it actually happens in other parts of the world. The reason for this is that the lack of logistical support in rural regions prevents the establishment and maintenance of instruments.

Four major dust episodes took place in spring 2001 around the following days: 1 to 6 March, 12 to 26 March, 4 to 20 April and 29 April to 5 May. Each dust event was always associated with a cold front outbreak. Also, some local dust events took place as evidenced by surface weather reports and observations from a network of ground-based aerosol sampling stations for China Dust Storm Research (ChinaDSR, Zhang et al., 2003). As shown in Fig. 3, the effect of these events on AODs was apparent in the time-series of AODs. During the first dust episode, most of the daily AODs in Kashi, Ulumuqi and Lanzhou exceeded the overall average. The most intense (in terms of magnitude and impacted area) and persistent dust episode occurred during 4 to 20 April, and was associated with high AODs at all stations; for example, the highest AODs in Ejinaqi occurred on 8 April with a value of 2.56. Corresponding to the fourth dust episode, daily AODs on 1 and 4 May in BJ were 2.96 and 2.60 respectively, being about four times greater than the overall average. Higher AODs also occurred at other sites during the fourth dust period. Generally, heavy aerosol loading and significant day-to-day variation (the overall average ranged from 0.32 in Ejinaqi to 0.68 in Beijing, with the averaged coefficient of variation (CV)

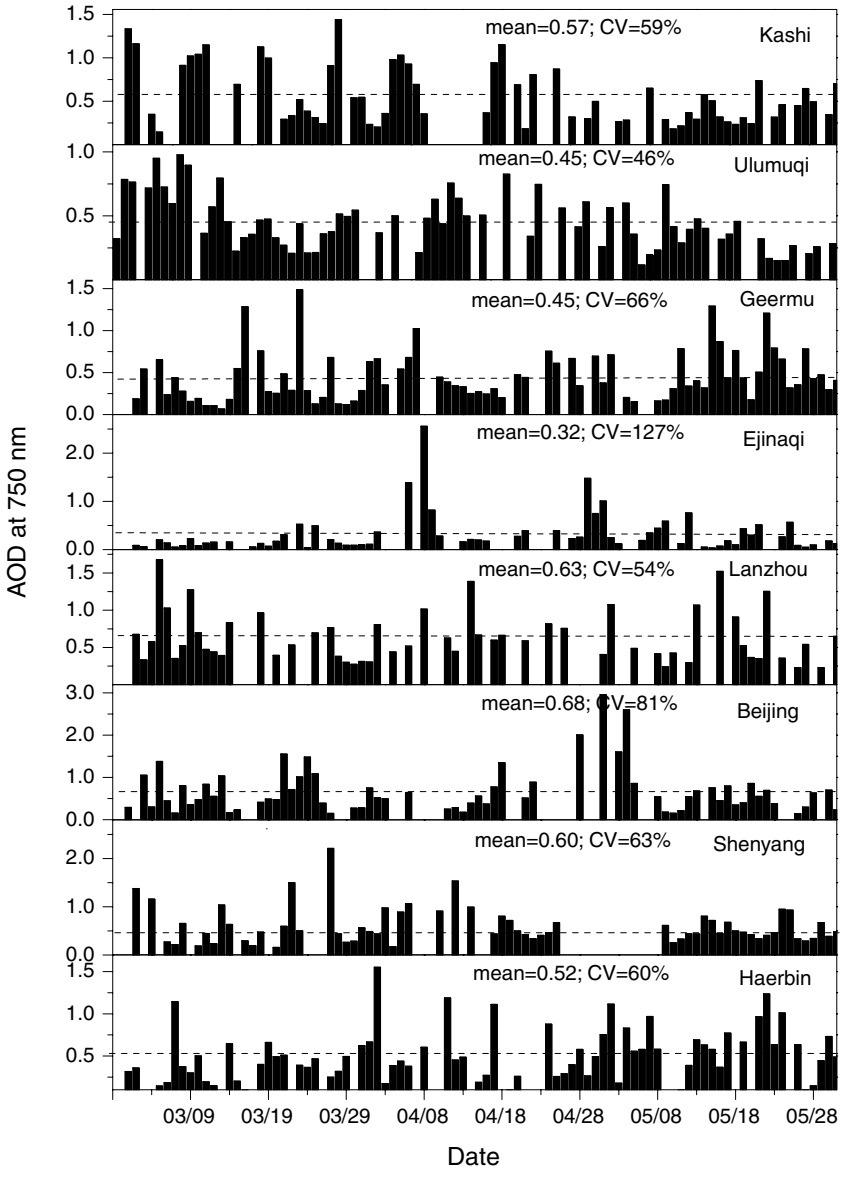

Fig 3. Time-series of daily aerosol optical depth (AOD) retrievals from the method of Qiu (2003) at eight radiation sites. The overall mean (dashed lines) and coefficient of variation for each site (CV = standard deviation/overall mean) are also presented.

being 70%) are evident in Fig. 3. This was mainly due to the effect of frequent dust outbreaks on AODs, but the contribution from anthropogenic pollution cannot be excluded. This will be demonstrated by the analysis of AERONET data in the following section. Also, dust properties over Chinese source regions and dust impacts on aerosol loading, size and absorption over downwind regions will be illustrated on the basis of AERONET data.

4. Aerosol properties at AERONET stations

4.1. AOD and ALPHA

Figure 4 shows the time-series of the daily average AOD at 500 nm (hereafter, AOD means aerosol optical depth at 500 nm unless otherwise indicated) and ALPHA. The overall mean and coefficient of the variation of AOD and ALPHA computed from all available daily averages are also presented in Fig. 4. Obviously, aerosol loading over northern China in spring was very high and varied over a wide range. The overall AOD average was 0.93 in DH, 0.81 in BJ, 0.69 in XH and 0.38 in IM. These values were comparable in magnitude to AODs in the Sahara and Sahel except in IM (Holben et al., 2001). The significant contribution of dust events to aerosol loading was confirmed by the frequent occurrence of a relatively low ALPHA, being less than 0.6. The impact of dust events on the aerosol loading at each station is described in detail in the following.

DH experienced three periods with higher AODs than the overall average, which were from 7 to 13 April, 19 to 21 April and 28 April to 1 May. High AODs were always associated with the dust

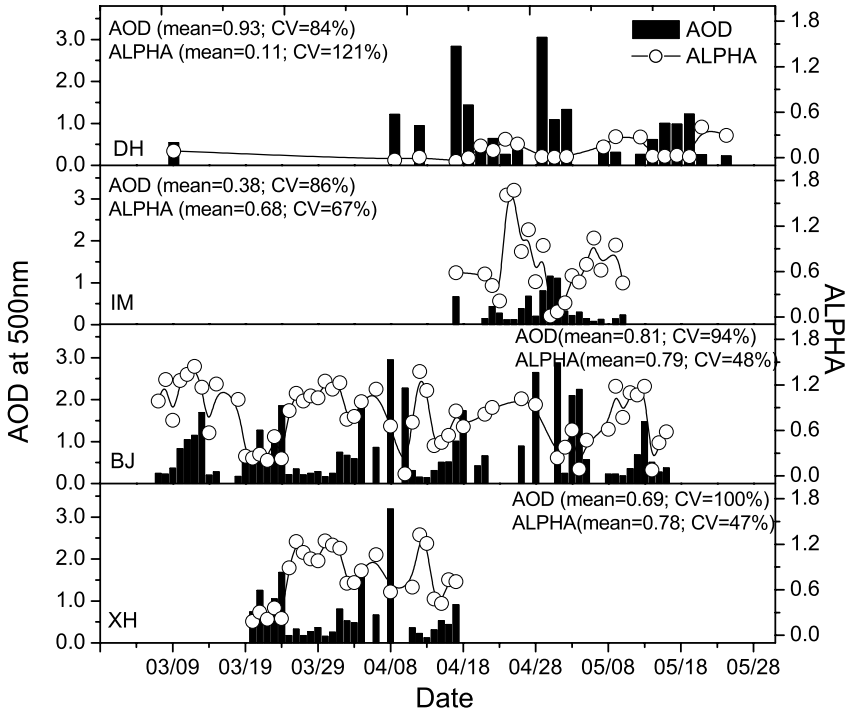

Fig 4. Time-series of daily aerosol optical depth (AOD) at 500 nm and Ångstrom wavelength parameter (ALPHA) at four AERONET sites. The overall average and coefficient of variation for each site are also presented.

event, which was confirmed by the surface weather reports and ALPHAs less than 0.1. The highest daily AOD exceeded 3.0 and occurred on 19 April; this was accompanied by an ALPHA close to zero. Dust events (probably depicted by AODs larger than the overall average and ALPHAs lower than 0.6) occurred in IM on 17 April and from 27 April to 2 May during the measurement period. But the highest daily AOD in IM was only about 1.16 this occurred on 30 April) and was much less than that in DH.

Note that AOD and ALPHA in BJ varied in a complicated manner. The AODs were relatively low and constant until about 10 March when they increased sharply; thereafter, the AODs remained quite high and were accompanied by ALPHAs higher than 1.0 until 14 March, then they returned to low values of about 0.2 in the subsequent five days. From 19 to 24 March, AODs increased from 0.52 to 1.85, and, contrarily, ALPHAs decreased from about 1.0 to 0.3, which was indicative of the occurrence of dust events in BJ. In the remaining days of March, AODs were relatively low and constant and ALPHAs were about 1.2. Then, AODs increased dramatically until 11 April when they returned to relatively low values; correspondingly, ALPHAs were relatively high at first and then decreased rapidly to nearly zero on 10 April, implying that BJ was seriously affected by the dust event on that day. Thereafter, the low turbidity did not last long and was followed by AODs persistently higher than the overall average with a combination of ALPHAs lower than 1.0 from 15 April to 5 May (suggesting BJ was seriously affected by both dust events and anthropogenic emissions during this period), although there were occasionally a few low AODs. Among the remaining measurements, most of the AODs were relatively low

Table 3. The four conditions of 'background', 'dust', 'mixed' and 'pollution', are classified according to aerosol optical depth (AOD) and Ångstrom wavelength parameter (ALPHA) in BJ

	AOD > 0.1		
AOD ≤ 0.1	ALPHA ≤ 0.25	0.25 < ALPHA < 1.0	ALPHA ≥ 1.0
Background	Dust	Mixed	Pollution

(around 0.2 at 500 nm) and ALPHAs were relatively high (>0.6). However, AODs from 12 to 14 May increased to about 1.5 and were accompanied by large ALPHAs (>1.0). According to the classification method suggested by Kubilay et al. (2003) on the basis of AOD and ALPHA (described in Table 3), there was only one case that reached the background level of aerosol in BJ; approximately 8% of the measurements might be attributed to pure dust cases; 54% belonged to mixed cases; and the remainder, i.e. 38%, were associated with dominant anthropogenic emissions. This indicates that dust aerosol is also the prevailing contributor to aerosol loading even in the metropolitan areas in spring over North China.

As shown in Fig. 4, there was good agreement in magnitude and variation of AOD and ALPHA in XH and BJ. This might be illustrated more clearly by the scatter plot between daily AOD and ALPHA in XH and BJ (see Fig. 5). The slopes of the linear regression were close to unity and the intercepts approached zero, with a correlation coefficient of 0.99. The fair agreement of AOD and ALPHA at these two stations occurred not only during

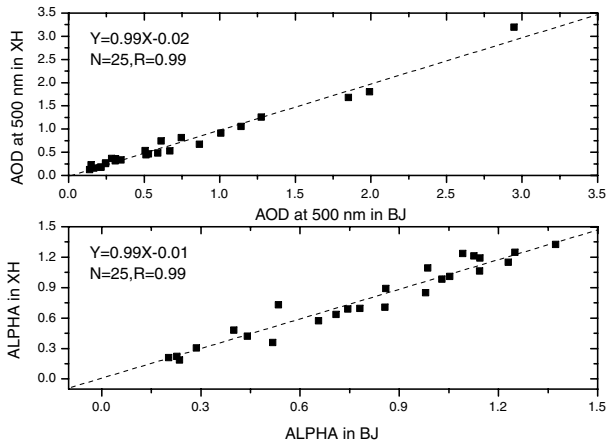

Fig 5. The linear regression analysis between daily aerosol optical depth (AOD) at 500 nm and Ångstrom wavelength parameter (ALPHA) in BJ and XH. The dashed lines represent a 1:1 relation.

the dust period (characterized by high AOD and low ALPHA), but also during the anthropogenic pollution period (characterized by high AOD and high ALPHA). In view of the distance of about 100 km from BJ to XH and the distinctly different environments surrounding BJ (urban region) and XH (rural region), the fair agreement of AOD and ALPHA is suggestive of the anthropogenic pollution, similar to the dust event, being on the regional scale. As a matter of fact, the moderate-resolution imaging spectroradiometer (MODIS) frequently remote sensed a thick shroud of haze that lingered over the North China Plain, turning the sky an opaque grey (http://rapidfire.sci.gsfc.nasa.gov).

The scatter plots of instantaneous AOD versus ALPHA are shown in Fig. 6. This visual representation often allows one to define physically interpretable cluster regions for different types of aerosols. Although no obvious cluster discrimination is evident, many features are worth noting. The largest spread occurred in BJ, showing that aerosols in BJ have the most complex sources and that each source produces aerosols with distinctly different properties. As seen in Fig. 6, even when AOD >2.0, ALPHA varied from nearly zero to approximately 1.2. This was due to the fact that BJ was affected not only by frequent dust events characterized by large particles but also by anthropogenic emissions characterized by fine particles. This will be verified by the analysis of aerosol size distribution retrievals in the next section. ALPHA in XH also exhibited a very complex relationship with AOD, but compared with that in BJ there was a little less spread of ALPHA at moderate to large values of AOD (>0.6) in XH. Contrary to the large spread in BJ and XH, there was much less spread in IM and DH, especially in DH, indicative of the relatively simple source in these regions. ALPHAs were close to zero and kept stable when AOD >0.6 in DH. For AOD <0.6, there was a significant negative correlation between ALPHA versus AOD, indicating the increasing contribution to AOD from large particles. A large spread of ALPHA, ranging from nearly zero to beyond 2, appeared only when AOD was <0.6 in IM. For AOD >0.6, most of the ALPHAs approached zero except for those on 27 and 29 April. A 3-day air mass back trajectory analysis (not shown) suggested that the air mass in the middle and low levels of the atmosphere travelled first in a westward direction and then veered dramatically in a northward direction toward IM; therefore, aerosols in IM for these days were probably mixed with the anthropogenic pollution transported from the southern industrial regions, which resulted in high AODs accompanied by relatively large ALPHAs. The fact that the overall ALPHA mean in IM is much larger than that in DH and comparable to that in BJ and XH also supports the hypothesis that anthropogenic emissions may have affected aerosol loading in IM on a few occasions in this period. Another notable difference between DH and IM was that there was a much larger variation in ALPHA for low AOD in IM, ranging from zero to beyond 2; as for DH, the majority of ALPHAs were below 0.6. Note that the occurrence frequency of background level of aerosols in IM (defined as AOD <0.10, Holben et al., 2001) is highest at approximately 14% (55 out of 393 observations); however, only one AOD out of 399 observations in DH is less than 0.1. Therefore, part of the reason for the wide range in ALPHAs for low AODs (especially for AODs <0.1) in IM was probably associated with the large errors in the computed ALPHAs when AODs were low.

4.2. Aerosol size distribution

Aerosol volume size distributions retrieved at four stations sorted by AOD are shown in Fig. 7. Each distribution was obtained by averaging nine to ten retrievals. The mean size distributions might be represented by the sum of two or three log-normal distributions as follows

$$v(r) = \frac{dV(r)}{d\ln r} = \sum_{i=1}^{n} \frac{C_{V,i}}{\sqrt{2\pi}\sigma_i} \exp\left(-\frac{(\ln r - \ln r_{v,i})^2}{2\sigma_i^2}\right) \quad 4.2.$$

where $v(r)$ is the volume size distribution, $C_{v,i}$ is the volume concentration per cross section of an atmospheric column, r is the aerosol radius, $r_{v,i}$ is the volume median radius and σ_i is the geometric standard deviation for each mode. In DH, the size distribution was composed of coarse particles with radii larger than 0.6 μm (up to 15 μm). The majority were concentrated around 2.0 μm and varied little. Large dust particles (>0.6 μm) contributed predominantly to AOD at 550 nm in DH. The value is about 68% (±5%) and close to that obtained in the Sahara and Saudi Arabia (Kaufman et al., 2002). The size distribution retrievals in BJ, XH and IM had three modes: one accumulation mode with mode radii of ~0.10 μm and two coarse modes with radii of near 1.30 and 3.80 μm. These two coarse modes were probably related to the occurrence of dust events.

Compared with retrievals in the mid-latitude sites (Dubovik et al., 2002b), $v(r)$ retrievals in BJ and XH had large fractions of coarse particles; for instance, the volume ratio of coarse

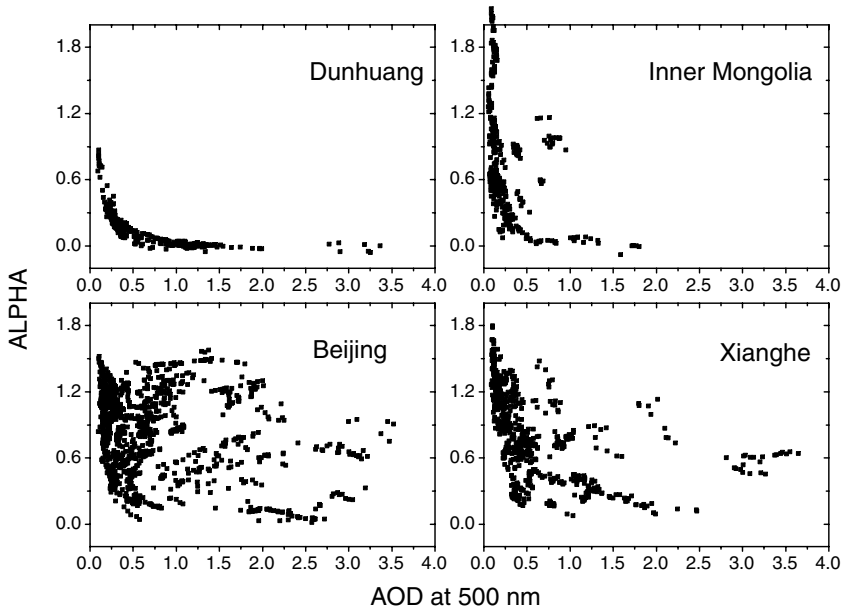

Fig 6. The scatter plots between instantaneous aerosol optical depth (AOD) at 500 nm and Ångstrom wavelength parameter (ALPHA) at four AERONET sites.

(>0.6 μm) to fine mode (<0.6 μm) in BJ was larger by a factor of ∼6 than that in Maryland and a Paris suburb (Dubovik et al., 2002b). This reflected the remarkable impact of the dust event on aerosol size in this period over northern China, which may be demonstrated clearly by $v(r)$ retrievals during the fourth dust period around 1 May. A cold front sweeping over North China began at the Chinese Taklimakan and Mongolian Gobi deserts on 29 April. One day later, an area of visibility <1 km was formed over the Onqin Daga Desert and further developed to cover Beijing during 1–7 May. Figure 10 presents daily $v(r)$ retrievals during this period. The columnar volume size concentrations for coarse particles in DH increased from 0.09 $\mu m^3\,\mu m^{-2}$ on 25 April to around 1.1 $\mu m^3\,\mu m^{-2}$ on 30 April; in IM, a nearly similar increase in coarse volume was observed. In BJ, the impact of the dust invasion on coarse volume was dramatic on 1 and 4 May, approaching 2.0 $\mu m^3\,\mu m^{-2}$; however, on 28 April and 3 May, the dust invasion and anthropogenic pollution contributed together to the high volume of coarse (about 0.85 $\mu m^3\,\mu m^{-2}$) and fine modes (about 0.25 $\mu m^3 \mu m^{-2}$), respectively. On 9 May, the size distribution retrieval finally returned to the background level.

In order to examine the effect of trajectories on aerosol size under different weather conditions, we computed 3-day back trajectories for four representative days (29 March, 17 April, 4 May, 13 May) using the hybrid single-particle Lagrangian integrated trajectory (HYSPLIT) model of the National Oceanic and Atmospheric Administration (NOAA; http://www.arl.noaa.gov/ready/hysp˙info.html), which are shown in Fig. 8. One day

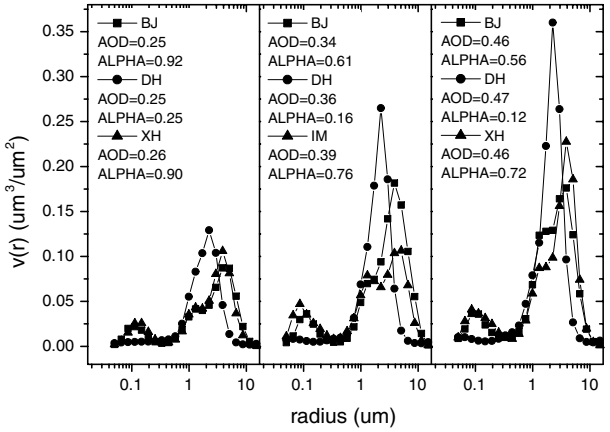

Fig 7. Aerosol size distribution retrievals sorted by aerosol optical depth (AOD) at four AERONET sites. The corresponding AODs and Ångstrom wavelength parameters (ALPHA) are also presented.

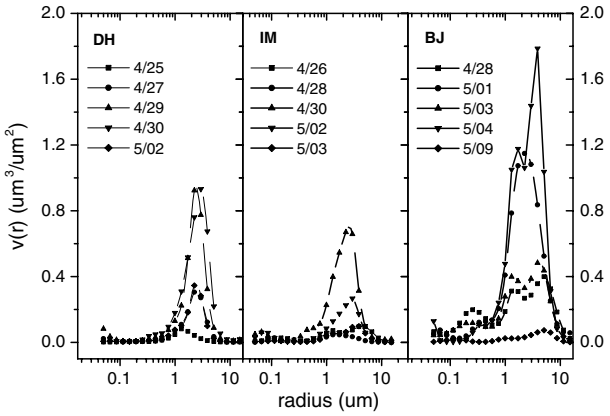

Fig 8. Aerosol size distribution retrievals in Dunhuang (DH), Inner Mongolia (IM), and Beijing (BJ) during a dust outbreak episode from 27 April to 7 May.

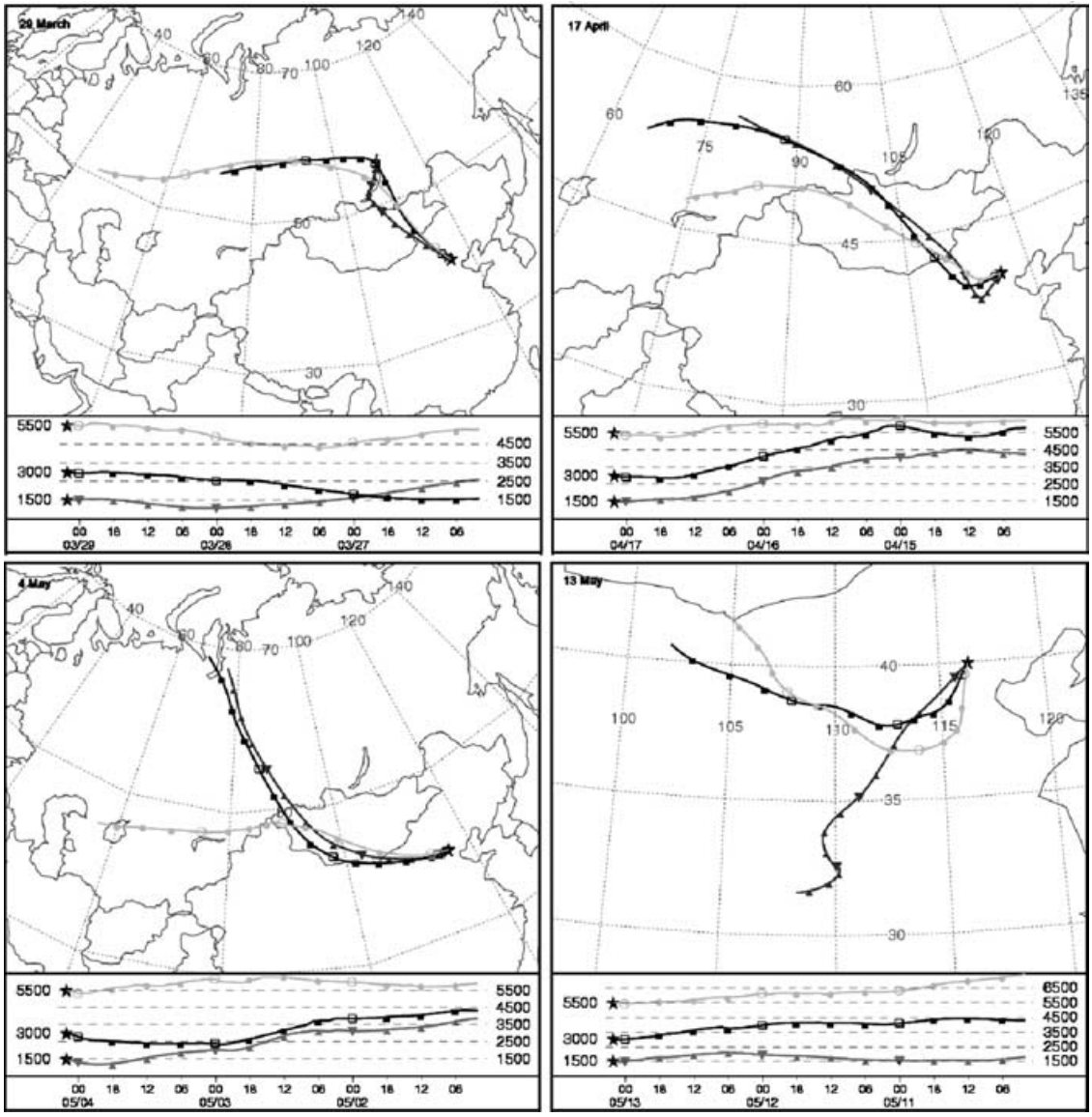

Fig 9. The 3-day back trajectory analyses corresponding to four distinctly different weather conditions in BJ: background (29 March), haze (17 April), dust (4 May) and light fog (13 May).

before 17 April and 13 May, the dominant airflow was from the southwestward direction, which indicated that anthropogenic aerosols from the industrial regions located to the south of BJ contributed to the high AODs in BJ. However, on 29 March and 4 May, the dominant airflow into BJ was directly from the west and northwest at all levels. According to the surface weather report, BJ was affected by a moderately strong dust storm around 4 May, whereas on 29 March no dust event occurred and the aerosol loading in BJ was relatively low. Figure 9 presents the corresponding aerosol size distribution retrievals. The relative shape of daily averaged size distributions on 17 April (haze) and 13 May (light fog) is similar to the retrieval on 29 March (probably representative of the background level of aerosols). The volume fraction of the fine mode ($r < 0.6\ \mu$m) was close to that of the coarse mode ($r > 0.6\ \mu$m); as a result, the high AODs for these 2 days were mainly a result of anthropogenic aerosols. The contribution from fine particles to AOD at 550 nm was 65 and 84% on 17 April and 13 May respectively and on 29 March it was 75%; these values are close to the retrieval in Mexico City (Kaufman et al., 2002). The domination of coarse particles was clearly demonstrated on 4 May, when a huge amount of desert dust accumulated in BJ, with the volume of coarse particles being an order in magnitude larger than that of the fine particles; hence, the principle contributor to high AOD was coarse particles (about 68% of AOD at 550 nm was attributed to coarse particles).

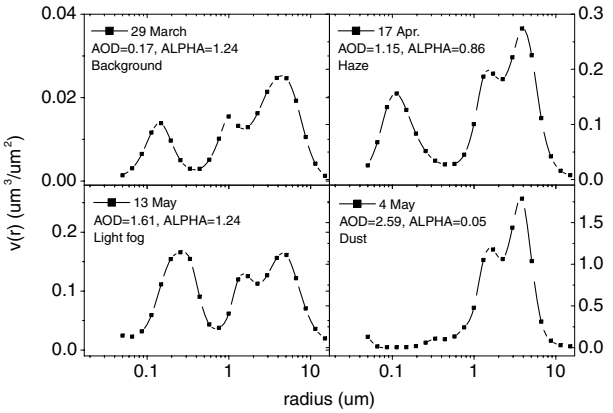

Fig 10. Aerosol size distribution retrievals corresponding to four distinctly different weather conditions in BJ: background (29 March), haze (17 April), dust (4 May) and light fog (13 May).

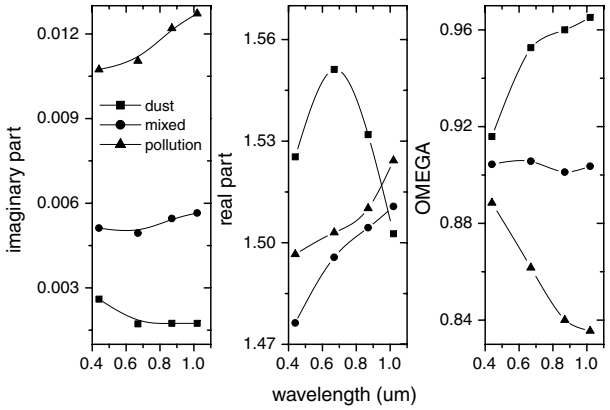

Fig 11. The average of refractive index and single-scattering albedo under three conditions: dust, mixed and pollution in BJ.

4.3. Refractive index and single-scattering albedo (OMEGA)

The dust absorption varied over a wide range as a function of the mineralogy of the aerosols. Desert aerosols in the Sahara, Sahel and their downwind regions were reported to have very low absorption (in the visible spectrum). This was revealed by a combination of satellite and surface retrievals (Kaufman et al., 2001). For the retrievals in DH, the averaged imaginary part of the refractive index was about 0.0008 and there was no wavelength dependence (actually, 22 imaginary parts out of 27 retrievals were close to 0.0005); as for OMEGA values, they increased from 0.97 at 0.44 μm to 0.99 at 1.02 μm (with 1 *SD* of about 0.01). The real part showed a little wavelength dependence, varying from 1.55 in the visible to 1.50 in the near infrared. The averaged imaginary part in IM was around 0.001 and had no wavelength dependence, but in fact 11 out of 17 retrievals were around 0.0005, which was the same as that in DH. The value 0.0005 was set to be the default minimum value in the algorithm that was indistinguishable from absolute zero. The real part in IM increased from about 1.48 at 0.44 μm to 1.54 at 1.02 μm. There was little difference in averaged OMEGAs between DH and IM. The retrieved imaginary part of the refractive index and single-scattering albedo suggested that pure dust over western China absorbs much less solar radiation than predicted by known aerosol models (Hess et al., 1998). The retrievals of the imaginary part and OMEGA in Chinese dust source regions were close to the minimum margin of ground-based and space-borne remote sensing results in other dust source regions (Kaufman et al., 2001; Dubovik et al., 2002b).

Figure 11 presents the averages of refractive index and OMEGA in BJ under conditions of dust, pollution and a mixture of both. It shows that both the magnitude and wavelength dependence of these properties were distinctly different under the three conditions. The imaginary part at 0.44 μm increased from around 0.002 during the dust outbreak episode to nearly 0.005 in the mixed case. As for the anthropogenic pollution period, it increased dramatically to approximately 0.010 and increased with the wavelength; however, during the dust episode, the imaginary part exhibited the opposite wavelength dependence, and had a nearly neutral wavelength dependence for the mixed case. The real part increased from 1.48 at 0.44 μm to about 1.52 at 1.02 μm for the mixed and anthropogenic pollution cases, but during the dust episode the real part increased within the range of 0.44–0.67 μm at first, and then decreased to within 0.67–1.02 μm. OMEGA exhibited the lowest values and decreased from 0.89 at 0.44 μm to 0.84 at 1.02 μm during the anthropogenic pollution episode; contrarily, the opposite wavelength dependence was observed for OMEGA (increasing from about 0.92 at 0.44 μm to around 0.97 at 1.02 μm) during the dust episode. As for the mixed case, OMEGA had little wavelength dependence, being around 0.90. On average, the imaginary part of the refractive index was 0.004 and OMEGA was around 0.90 and showed little spectral dependence in BJ. Compared with AERONET retrievals in other regions, the imaginary part and OMEGA in BJ were intermediate between that in Maryland (weak absorption) and Mexico City (strong absorption). Actually, as shown in Fig. 11, aerosol absorption (the magnitude and spectral dependence) in BJ was seriously affected by the dust outbreak. The averages of the imaginary part and OMEGA retrieved for the anthropogenic pollution case were very similar to retrievals in Mexico City and the Maldives (Dubovik et al., 2002b). Combined with the similarity in aerosol size distribution retrievals, the contribution of the absorption to total AOD (12.5%) in BJ for the anthropogenic pollution case is also similar to that in Mexico City and the Maldives (Kaufman et al., 2002). As for the dust period in BJ, the aerosol absorption contributed to only about 6% of AOD. The estimation of OMEGA at 0.55 μm by Bergin et al. (2001) in BJ was 0.81 at a relative humidity of 40% in summer 1999, which was derived by analysis of ground samples. According to the retrievals of laser and sun-photometer measurements in BJ, the values of OMEGA at 0.65 μm were reported to be 0.72 and 0.85 respectively prior to and during a dust outbreak period in

spring 1988 (Qiu and Sun, 1994). The fact that OMEGA showed a significant increase with the dust invasion as suggested by Qiu and Sun (1994) was consistent with our analysis. The potential reason for the decrease of OMEGA during the dust period is the input of a large volume of dust aerosols with relatively lower absorption compared with anthropogenic aerosols. Note that both the Bergin et al. (2001) and Qiu and Sun (1994) derivations of OMEGA were derived only from case studies. The derivations were within the range of AERONET retrievals, but they approached the minimum value.

5. Conclusions and discussion

On the basis of aerosol properties from AERONET retrievals and aerosol optical depth at 750 nm retrieved from DSR data over North China in spring 2001, we studied the spatial and temporal variation of aerosol loading, size and absorption. The impact of the dust events on aerosol loading and properties was revealed based mainly on aerosol data at AERONET stations. To our knowledge this is the first time that such a simultaneous ground-based remote sensing of aerosols in Chinese dust source and downwind regions has been reported.

Heavy aerosol loading and large temporal variation over North China was revealed. The AOD at 750 nm at eight radiation stations was around 0.53. The coefficient of variation of AOD ranged from 46% at Ulumuqi to 127% at Ejinaqi. Large dust particles (>0.6 μm) contributed predominantly to AOD over western China, the contribution being about 68% ($\pm 5\%$). However, in the downwind urban and rural regions, anthropogenic emissions and sporadic dust outbreaks each made a contribution to the heavy aerosol loading. The fingerprint of the dust event on the aerosol loading in BJ was evident, and more than 60% of measurements were associated with a dust event more or less according to the classification on the basis of Ångstrom wavelength exponent. The dramatic increase in AOD at 500 nm from $\sim$0.1 to a high value of $\sim$4 was observed in BJ, which was accompanied by a simultaneous decrease of Ångstrom wavelength exponent from more than unity to nearly zero during the dust period. A similar increase in AOD, but associated with higher values than unity and less variation of Ångstrom wavelength exponent, was also observed on a few occasions, which implied a dramatic effect of anthropogenic pollution. The fraction of AOD due to coarse particles in BJ increased rapidly from about 30% (at 550 nm) for the anthropogenic pollution case to values like those in DH during the dust period.

Pure dust aerosols in Chinese dust source regions have much less absorption in the visible spectrum than estimated from the aerosol models, but they are in agreement with the ground or satellite remote sensing result in other dust source regions.

The similarity in magnitude and temporal variation of AOD and the Ångstrom wavelength exponent in BJ and XH, although the two sites are separated by about 100 km, implied anthropogenic pollution; similar to the dust event, this was also on a regional scale.

The properties such as size and absorption of dust and anthropogenic aerosol were distinctly different. Dust aerosol mainly comprised coarse particles with negligible absorption in the visible spectrum; contrarily, anthropogenic aerosol showed absolutely the opposite characteristics. The aerosol absorption in BJ during the periods without the dust invasion was similar to the retrievals in the urban regions such as in Mexico City and the Maldives and much stronger than that in Maryland. The input of a large volume of dust aerosols with a negligible absorption during the dust period resulted in a remarkable decrease in the aerosol absorption. Aerosol absorption is one of the key properties determining the effect of aerosols on the climate. Strong aerosol absorption can lead to a large difference in aerosol forcing at the top of the atmosphere and at the Earth's surface, which results in a significant increase in solar radiation absorption in the atmosphere, accordingly raising some intriguing scientific questions that are concerned with the global and regional circulation, temperature change and the hydrological cycle (Satheesh and Ramanathan 2000; Ramanathan et al., 2001). A few preliminary studies argued that the general increasing trend of aerosols with strong absorption over southeast China could affect crop yields and contribute to the trend of a climate change pattern of northern drought and southern flooding (Menon et al., 2002; Chameides et al., 1999). Consequently, the impact of dust outbreaks on aerosol absorption leading to climate effects in downwind regions warrant greater attention.

6. Acknowledgments

The authors thank Professors B. N. Holben and D. R. Lu for establishing four AERONET stations over North China and providing data. We would like to thank the NOAA Air Resources Laboratory team for providing the HYSPLIT_4 trajectory model run on-line. We are grateful to the anonymous reviewers for their constructive comments and Mr B. Daren for his help in modifying the English. This research was funded as a part of the NSFC grants 40305002, 40175008, 40333029 and the NSFC Overseas Cooperation Foundation grant 40028503.

References

Bergin, M. H., Cass, G. R., Xu, J., Fang, C., Zeng, L. M. et al., 2001. Aerosol radiative, physical and chemical properties in Beijing during June 1999. *J. Geophys. Res.* **106**, 17 969–17 980.

Chameides, W. L., Yu, H., Liu, S. C., Bergin, M. H., Zhou, X. et al. 1999. Case study of the effects of atmospheric aerosols and regional haze on agriculture: An opportunity to enhance crop yields in China through emission controls?. *Proc. Natl. Acad. Sci., USA* **26**, 13 626–13 633.

Dubovik, O., Holben, B. N., Eck, T. F., Smirnov, A., Kaufman, Y. J. et al. 2002b. Variability of absorption and optical properties of key aerosol types observed in worldwide locations. *J. Atmos. Sci.* **39**, 590–608.

Dubovik, O., Holben, B. N., Lapyonok, T., Sinyuk, A., Mishchenko, M. I. et al. 2002a. Non-spherical aerosol retrieval method employing light scattering by spheroids. *Geophys. Res. Lett.* **29**(10), doi:10.1029/2001GL014506.

Dubovik, O., Smirnov, A., Holben, B. N., King, M. D., Kaufman, Y. J. et al. 2000a. Accuracy assessments of aerosol optical properties retrieved from AERONET sun and sky radiance measurements. *J. Geophys. Res.* **105**, 9791–9806.

Dubovik, O., Smirnov, A., Holben, B. N., King, M. D., Kaufman, Y. J. et al. 2000b. Accuracy assessments of aerosol optical properties retrieved from AERONET sun and sky radiance measurements. *J. Geophys. Res.* **105**, 9791–9806.

Eck, T. F., Holben, B. N., Ward, D. E., Mukelabai, M. M., Dubovik, O. et al. 2003. Variability of biomass burning aerosol optical characteristics in southern Africa during the SAFARI 2000 dry season campaign and a comparison of single scattering albedo estimates from radiometric measurements. *J. Geophys. Res.* **108**(D13), 8477, doi:10.1029/2002JD002321.

Hess, M., Koepke, P. and Schult, I. 1998. Optical properties of aerosols and clouds: the software package OPAC. *Bull. Am. Meteorol. Soc.* **79**, 831–844.

Holben, B. N., Eck, T. E., Slutsker, I., Tanre, D., Buis, J. P. et al. 1998. AERONET—a federated instrument network and data archive for aerosol characterization. *Remote Sens. Environ.* **66**, 1–16.

Holben, B. N., Tanre, D., Smirnov, A., Eck, T. F., Slutsker, I. et al. 2001. An emerging ground-based aerosol climatology: aerosol optical depth from AERONET. *J. Geophys. Res.* **106**, 12 076–12 097.

Intergovernmental Panel on Climate Change (IPCC), 2001. *Climate Change 2001: The Scientific Basis—Contribution of Working Group I to the Third Assessment Report of the Intergovernmental Panel on Climate Change*. Cambridge University Press, New York.

Kaufman, Y. J., Tanre, D. and Boucher, O. 2002. A satellite view of aerosols in the climate system. *Nature* **419**, 215–223.

Kaufman, Y. J., Tanre, D., Dubovik, O., Karnieli, A. and Remer, L. A. 2001. Absorption of sunlight by dust as inferred from satellite and ground-based remote sensing. *Geophys. Res. Lett.* **28**, 1479–1482.

Kubilay, N., Cokacar, T. and Oguz, T. 2003. Optical properties of mineral dust outbreaks over the northeastern Mediterranean. *J. Geophys. Res.* **108**(D21), 4666, doi:10.1029/2003JD003798.

Menon, S., Hansen, J., Nazarenko, L. and Luo, Y. F. 2002. Climate effects of black carbon aerosols in China and India. *Science* **297**, 2249–2252.

Pinker, R. T., Pandithurai, G., Holben, B. N., Dubovik, O. and Aro, T. O. 2001. A dust outbreak episode in sub-Sahel west Africa. *J. Geophys. Res.* **106**, 22 923–22 930.

Qiu, J. H. 1998. A method to determine atmospheric aerosol optical depth using total direct solar radiation. *J. Atmos. Sci.* **55**, 744–757.

Qiu, J. H. 2003. Broadband extinction method to determine aerosol optical depth from accumulated direct solar radiation. *J. Appl. Meteorol.* **42**, 1611–1625.

Qiu, J. H. and Sun, J. H. 1994. Optically remote sensing of the dust storm and result analysis. *Sci. Atmos. Sinica* **18**, 1–10.

Ramanathan, V., Crutzen, P. J., Kiehl, J. T. and Rosenfeld, D. 2001. Aerosols, climate, and the hydrological cycle. *Science* **294**, 2119–2124.

Satheesh, S. K. and Ramanathan, V. 2000. Large differences in tropical aerosol forcing at the top of the atmosphere and Earth's surface. *Nature* **405**, 60–63.

Smirnov, A., Holben, B. N., Eck, T. F., Dubovik, O. and Slutsker, I. 2000. Cloud screening and quality control algorithms for the AERONET database. *Remote Sens. Environ.* **73**, 337–349.

Smirnov, A., Holben, B. N., Kaufman, Y. J., Dubovik, O., Eck, T. E. et al. 2002. Optical properties of atmospheric aerosol in maritime environments. *J. Atmos. Sci.* **59**, 484–500.

Wang, M. X., Zhang, R. J. and Pu, Y. F. 2001. Recent researches on aerosol in China. *Adv. Atmos. Sci.* **18**, 576–586.

Xu, J., Bergin, M. H., Yu, X., Liu, G., Zhao, J. et al. 2002. Measurement of aerosol chemical, physical and radiative properties in the Yangtze delta region of China. *Atmos. Environ.* **36**, 161–173.

Zhang, J. H., Mao, J. T. and Wang, M. H. 2002. Analysis of aerosol extinction characteristics in different areas of China. *Adv. Atmos. Sci.* **19**, 136–152.

Zhang, X. Y., Gong, S. L., Shen, Z. X., Mei, F. M., Xi, X. X. et al. 2003. Characterization of soil dust aerosol in China and its transport and distribution during 2001 ACE-Asia: 1. Network observations. *J. Geophys. Res.* **108**(D9), 4261, doi:10.1029/2002JD002632.